$RE_{2+x}I_2M_{2+y}$ (RE = Ce, Gd, Y; M = Al, Ga): Reduced Rare Earth Halides with a Hexagonal Metal Atom Network

Mar'yana Lukachuk[a], Chong Zheng[b], Hansjürgen Mattausch[a], Michael G. Banks[a], Reinhard K. Kremer[a], and Arndt Simon[a]

[a] Max-Planck-Institut für Festkörperforschung, Heisenbergstraße 1, D-70569 Stuttgart, Germany
[b] Department of Chemistry and Biochemistry, Northern Illinois University, DeKalb, IL 60115, USA

Reprint requests to C. Zheng and A. Simon.
E-mail: zheng@cz.chem.niu.edu and A.Simon@fkf.mpg.de

Z. Naturforsch. **2007**, *62b,* 633 – 641; received October 23, 2006

The title compounds were synthesized from RE, REI_3 (RE = Ce, Gd, Y) and Al or Ga under an Ar atmosphere at 930 – 950 °C. The non-stoichiometric $Ce_{2+x}I_2Al_{2+y}$ and $Ce_{2+x}I_2Ga_{2+y}$ compounds crystallize in the space group $R\bar{3}m$ (No. 166) with lattice constants a = 4.3645(3), c = 35.914(2) Å for the Al and a = 4.3009(2), c = 35.680(4) Å for the Ga compound. Excess electron density found in the Wyckoff position 3a could be due to a fractional occupation by Ce or M (x = 0.06, y = 0 or x = 0, y = 0.11 in the case of the Ga compound). The stoichiometric $Gd_2I_2Ga_2$ and $Y_2I_2Ga_2$ compounds crystallize in the space group $P\bar{3}m1$ (No. 164) with lattice constants a = 4.1964(1) and 4.1786(7) Å, c = 11.4753(4) and 11.434(2) Å, respectively. Their structures feature M-centered (M = Al, Ga) RE trigonal prisms condensed *via* common rectangular faces. The electronic origin of the surplus of metal atoms in the octahedral voids between the I-layers of the Ce compounds was explored *via* extended Hückel-type calculations. Magnetic susceptibility, electrical resistivity and heat capacity measurements have also been carried out. These reveal a metal-insulator transition of $Gd_2I_2Ga_2$ at 40 K.

Key words: Cerium, Gadolinium, Yttrium, Aluminum, Gallium, Reduced Halide

Introduction

Reduced rare earth metal halides have demonstrated extremely rich chemistry and structural variations [1 – 4]. They typically have metal octahedra or trigonal prisms as their building units [5 – 9]. These polyhedra usually contain a third element at their centers. In the case of trigonal prism based structures, these units as a rule condense into two-dimensional layers by sharing their common rectangular faces. As a result, the element that centers the trigonal prisms can form a two-dimensional extended network of triangular, pentagonal, hexagonal or even octagonal rings [2, 10, 11]. The honeycomb network is particularly interesting, as it can be planar or puckered depending on its environment and electronic configuration [12]. In this contribution, we report four new compounds of this type.

Experimental Section

Synthesis

RE metals (RE = Ce, Gd, Y) (sublimed, 99.99 %; Alfa-Aesar, small pieces), REI_3 and Al or Ga (99.99 %; Aldrich) were used as starting materials. CeI_3 was synthesized from the reaction of Ce metal with I_2. GdI_3 and YI_3 were prepared from the reaction of the oxides (99.9 %) with HI and NH_4I. REI_3 were purified twice by sublimation in a Ta tube before being used. Due to the air and moisture sensitivity of the starting and product materials, all handling was carried out under Ar atmosphere either in a glovebox or through standard Schlenk technique.

The mixtures ($\sim$ 1 g) of the starting materials in an atomic ratio 1 : 1 : 1 were arc-sealed in Ta tubes under an Ar atmosphere. The Ta tubes were then sealed into silica glass ampoules under a vacuum of *ca.* 10^{-2} mbar. The reaction temperature 930 °C was kept 15 days for Ce/I/Al, 10 days for Ce/I/Ga, and 15 days for $Gd_2I_2Ga_2$. $Y_2I_2Ga_2$ was prepared at 950 °C (10 days). A powder sample of $Tb_2I_2Ga_2$ was also prepared at the same reaction conditions as for $Gd_2I_2Ga_2$. Its powder X-ray pattern showed that it is isostructural to $Gd_2I_2Ga_2$ with lattice constants a = 4.1807(7) and c = 11.438(3) Å. However, the sample contained some oxide halide according to its Guinier pattern.

After the reactions, the ampoules were opened under Ar atmosphere. Many metallic golden thin platelets were observed in the products (Fig. 1). The yield, estimated from Guinier measurements, was greater than 90 %. EDX analyses

Table 1. Crystal data and structure refinement for $Ce_{2.29}I_2Al_2$, $Ce_{2+x}I_2Ga_{2+y}$ and $Y_2I_2Ga_2$.

Empirical formula	$Ce_{2.29}I_2Al_2$	$Ce_{2.06}I_2Ga_2$ ($CeI_2Ga_{2.11}$)	$Y_2I_2Ga_2$
Formula weight	629.10	681.89	571.06
Temperature [K]	293(2)	293(2)	293(2)
Wavelength [Å]	0.56086	0.71073	0.71073
Crystal system	rhombohedral	rhombohedral	trigonal
Space group	$R\bar{3}m$ (No. 166)	$R\bar{3}m$ (No. 166)	$P\bar{3}m1$ (No. 164)
Unit cell dimensions [Å] a:	4.3645(3)	4.3009(2)	4.1786(7)
c:	35.914(2)	35.680(4)	11.434(2)
Volume [Å^3], Z	592.46(6), 3	571.57(7), 3	172.91(5), 1
D_{calc} [g cm^{-3}]	5.29	5.94	5.48
Absorption coefficient [mm^{-1}]	11.09	27.04	33.12
Transm. ratio (max/min)	1.19	4.81	5.92
$F(000)$ [e]	795	862	246
θ range for data collection [deg]	2.69 – 23.92	5.50 – 29.96	3.56 – 27.44
Index ranges	$0 \le h \le 6$	$-5 \le h \le 6$	$-5 \le h \le 5$
	$-6 \le k \le 0$	$-6 \le k \le 6$	$-5 \le k \le 5$
	$-51 \le l \le 51$	$-50 \le l \le 50$	$-14 \le l \le 14$
Reflections collected	994	1623	1473
Independent data / parameters	291 / 14	246 / 14	194 / 11
Goodness-of-fit on F^2	1.231	1.195	1.165
$R1/wR2$[a] [$I \ge 2\sigma(I)$]	0.0186 / 0.0496	0.0216 / 0.0646	0.0268 / 0.0572
$R1/wR2$[a] (all data)	0.0192 / 0.0499	0.0220 / 0.0648	0.0289 / 0.0577
Largest diff. peak / hole [e Å^{-3}]	1.363 / −1.044	2.463 / −1.292	1.939 / −0.960

[a] $R1 = \Sigma||F_o| - |F_c||/\Sigma|F_o|$; $wR2 = [\Sigma[w(F_o^2 - F_c^2)^2]/\Sigma[w(F_o^2)^2]]^{1/2}$.

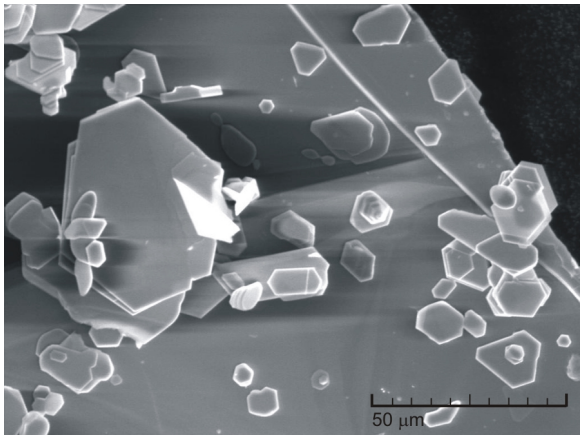

Fig. 1. SEM image of $Ce_{2+x}I_2Ga_{2+y}$ crystals.

of single crystals, using a TESCAN scanning electron microscope with an Oxford EDX detector, confirmed the presence of the component elements in the average atomic ratio of 1 : 1 : 1 with a possible experimental error of approximately 10 %.

Structure determination

The reaction products were ground to fine powders under an Ar atmosphere and sealed in glass capillaries for phase identification by a modified Guinier technique [13] (Cu$K_{\alpha 1}$: λ = 1.54056 Å; Si as internal standard with a = 5.43035 Å; Fujifilm BAS-5000 image plate system). Single crystals of the Y and Ce compounds were transferred to glass capillaries under Na-dried paraffin oil and sealed under Ar atmosphere.

Table 2. Crystal data and Rietveld structure refinement for $Gd_2I_2Ga_2$.

Empirical formula	$Gd_2I_2Ga_2$
Formula weight	353.88
Temperature [K]	293(2)
Wavelength [Å]	0.71073
Crystal system	trigonal
Space group	$P\bar{3}m1$ (No. 164)
Unit cell dimensions [Å] a:	4.1964(1)
c:	11.4753(4)
Volume [Å^3], Z	175.00(1), 1
D_{calc} [g cm^{-3}]	6.72
Number of collected points (N)	5800
Number of reflections	272
Number of refined parameters (P)	14
S	2.51
R_p / R_{wp} / R_{exp}	0.0603 / 0.0799 / 0.0319

They were first examined by the precession technique before being characterized on a Bruker CCD or a Stoe IPDSII diffractometer. The structures were solved with Direct Methods using the SHELXS and SIR97 programs [14, 15]. Full-matrix least-squares refinement on F^2 was carried out using SHELXTL [14]. The structure of the Gd compound was determined by powder diffraction data based on the Rietveld profile refinement method using FullProf [16].

$Ce_{2+x}I_2Al_{2+y}$ and $Ce_{2+x}I_2Ga_{2+y}$ crystallize in the rhombohedral space group $R\bar{3}m$ (No. 166) with Z = 3, whereas $Gd_2I_2Ga_2$ and $Y_2I_2Ga_2$ crystallize in $P\bar{3}m1$ (No. 164) with Z = 1. The crystallographic information including the fractional coordinates and interatomic distances of these compounds is listed in Tables 1 to 5. Further details on the crystal structure investigation are available.

Table 3. Atomic coordinates and equivalent isotropic displacement parameters ($Å^2 \times 10^3$) for $Ce_{2.29}I_2Al_2$, $Ce_{2.06}I_2Ga_2$ ($Ce_2I_2Ga_{2.11}$) and $Y_2I_2Ga_2$. U(eq) is defined as one third of the trace of the orthogonalized U_{ij} tensor.

Atom	Wyckoff position	x/a	y/b	z/c	U(eq)	sof
$Ce_{2.29}I_2Al_2$ ($R\bar{3}m$)						
Ce	6*c*	1/3	2/3	0.10795(1)	11(1)	1
I	6*c*	2/3	1/3	0.04822(1)	20(1)	1
Al	6*c*	0	0	0.16296(6)	11(1)	1
Ce1	3*a*	0	0	0	33(1)	0.29
$Ce_{2.06}I_2Ga_2$ ($Ce_2I_2Ga_{2.11}$) ($R\bar{3}m$)						
Ce	6*c*	1/3	2/3	0.10722(1)	10(1)	1
I	6*c*	2/3	1/3	0.04823(2)	15(1)	1
Ga	6*c*	0	0	0.15863(3)	10(1)	1
Ce1 (Ga1)	3*a*	0	0	0	30(5)	0.06 (0.11)
$Y_2I_2Ga_2$($P\bar{3}m1$)						
Y	2*c*	0	0	0.1771(1)	12(1)	1
I	2*d*	1/3	2/3	0.3509(1)	16(1)	1
Ga	2*d*	2/3	1/3	0.0292(1)	12(1)	1

Details may be obtained from Fachinformationszentrum Karlsruhe, 76344 Eggenstein-Leopoldshafen, Germany (Fax: +49-7247-808-666; e-mail: crysdata@fiz-karlsruhe.de, http://www.fiz-informationsdienste.de/en/DB/icsd/depot_anforderung.html) on quoting the deposition numbers CSD-417147 ($Ce_{2.29}I_2Al_2$), CSD-417148 ($Ce_{2.06}I_2Ga_2$), and CSD-417149 ($Y_2I_2Ga_2$).

Computational study

The density of states (DOS) and the crystal orbital overlap population (COOP) [17] curves were computed using both the tight-binding extended Hückel method (EH) [18, 19] and the self-consistent linear muffin-tin orbital density functional scheme using the local density approximation (LDA) as implemented in the Stuttgart-TB-LMTO-ASA program [20]. The electron localization function (ELF) [21 – 28] was also calculated using the LDA method. Approximately 500 k points in the irreducible wedge of the Brillouin zone were used in the EH computation of the DOS and COOP curves. More than 1000 k points in the whole Brillouin zone were generated in the LDA calculations. These k points were then reduced to the irreducible wedge of the Brillouin zone. The EH parameters used in the computation are listed in Table 6.

Physical property measurements

For conductivity measurements, the polycrystalline samples were pressed into pellets of 5 mm in diameter and *ca.* 2 mm thickness. The conventional four-point van-der-Pauw method [29] was used to measure the resistivities. The magnetic susceptibilities were determined with a MPMS SQUID magnetometer (Quantum Design) using sample quantities of *ca.* 50 mg. The heat capacities were measured with a PPMS 6000 system (Quantum Design) on samples of *ca.* 20 mg ($Gd_2I_2Ga_2$ and $Y_2I_2Ga_2$) and with the *quasi*-adiabatic step-heating method (Nernst's method) on a powder sample of *ca.* 0.4 g, which was encapsulated in a glass ampoule under 1 bar He gas to ensure thermal coupling. The heat capacity of the glass ampoule was determined in a separate run and subtracted in the case of $Ce_{2+x}I_2Ga_{2+y}$ [30].

Table 4. Atomic coordinates and equivalent isotropic displacement parameters ($Å^2 \times 10^3$) for $Gd_2I_2Ga_2$.

Atom	Wyckoff position	x/a	y/b	z/c	U(eq)
Gd	2*c*	0	0	0.1790(1)	3(1)
I	2*d*	1/3	2/3	0.3532(2)	5(1)
Ga	2*d*	2/3	1/3	0.0244(3)	10(1)

Table 5. Selected interatomic distances (Å) and angles (deg) for $RE_{2+x}I_2M_{2+y}$ (*RE* = Ce, Gd, Y; *M* = Al, Ga).

		$Ce_{2.29}I_2Al_2$	$Ce_{2.06}I_2Ga_2$ ($Ce_2I_2Ga_{2.11}$)
Ce–*M*	(×3)	3.202(1)	3.0871(7)
Ce–$M^{\#4}$	(×3)	3.373(1)	3.4588(8)
Ce–I	(×3)	3.3092(4)	3.2552(5)
Ce1(*M*1)–I	(×6)	3.0576(3)	3.0211(3)
M–$M^{\#4}$	(×3)	2.5339(5)	2.5485(5)
$M^{\#4}$–*M*–$M^{\#6}$	(×3)	118.91(3)	115.09(3)
		$Y_2I_2Ga_2$	$Gd_2I_2Ga_2$
RE–Ga	(×3)	2.947(1)	3.003(2)
	(×3)	3.374(2)	3.364(3)
RE–I	(×3)	3.125(1)	3.141(2)
Ga–Ga	(×3)	2.5030(9)	2.487(1)
Ga–Ga–Ga	(×3)	113.18(6)	115.08(4)

Symmetry transformations used to generate equivalent atoms: $^{\#4}$ $-x+2/3, -y+1/3, -z+1/3$; $^{\#6}$ $-x-1/3, -y+1/3, -z+1/3$.

Table 6. Extended Hückel parameters.

	Orbital	H_{ii} (eV)	ζ_1[a]	ζ_2	c_1[a]	c_2
Ce	6*s*	−4.97	1.799			
	6*p*	−4.97	2.20			
	5*d*	−6.43	3.90	2.10	0.7765	0.4586
I	5*s*	−18.0	2.679			
	5*p*	−12.7	2.322			
Ga	4*s*	−14.58	1.77			
	4*p*	−6.75	1.55			

[a] Exponents and coefficients in a double ζ expansion of the *d* orbital.

Results and Discussion

Crystal structures

$Ce_{2+x}I_2Al_{2+y}$ and $Ce_{2+x}I_2Ga_{2+y}$ are isostructural to $Y_2Br_2Fe_{2+x}$ and feature Al and Ga centered Ce trigonal prisms, respectively, condensed into two-dimensional layers propagating in the *a* and *b* directions (Fig. 2) [31]. These layers stack along the *c* axis with the I atoms between them. The sequence of each layer I-Ce-(*MM*)-Ce-I follows a close-packing pattern *cA(bc)Ab*. In the layer below, the first I atom sheet then

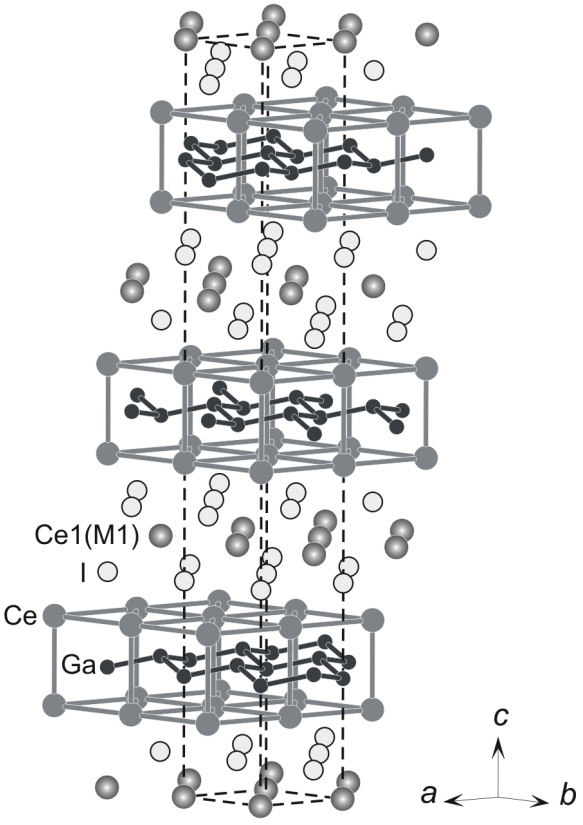

Fig. 2. The $Ce_{2+x}I_2M_{2+y}$ (M = Al, Ga) structure viewed approximately along [110]. It consists of three I-Ce-(*MM*)-Ce-I layers per unit cell. The Ce1(*M*1) atoms reside in the octahedral voids between two I sheets.

shifts to the *a* position, and the layer packing becomes *aB(ca)Bc*. In the second layer below, the sequence is *bC(ab)Ca*, and the pattern then repeats itself. Within a layer, the Al or Ga atoms connect to form a two-dimensional honeycomb net which is slightly puckered with an Al–Al–Al angle of 118.9° and a Ga–Ga–Ga angle of 115.1°. The Al–Al and Ga–Ga distances are 2.5339(5) and 2.5485(5) Å, respectively. These are comparable to the sum of covalent radii of two Al (2×1.25 Å in Pauling scale) or Ga atoms (2×1.26 Å). The shortest Ce–Ce distances are 4.217 and 4.242 Å in the Al and Ga compounds along the rectangular edge of the Ce_6 trigonal prism.

In the structure refinement significant excess electron density is found in Wyckoff site 3*a*, *i.e.* at the centers of the trigonal antiprisms formed by the I atoms. The distances from the centers to the adjacent I atoms are 3.058 and 3.021 Å in the Al- and Ga-containing compounds, respectively. In the isostructural compound $Y_2Br_2Fe_{2+x}$ the corresponding excess scattering density has been assigned unambiguously to additional Fe atoms by XPS measurements [31]. Refinement of the Al-containing compound as $Ce_2I_2Al_{2+y}$ resulted in an unreasonable value $y = 1.29$. With Ce in the position 3*a* the structure refined as $Ce_{2.29}I_2Al_2$. Alternative refinements of the Ga-containing compound as either $Ce_{2.06}I_2Ga_2$ or $Ce_2I_2Ga_{2.11}$ converged to only marginally different R values. The slightly increased magnetic moment (*vide infra*) is in fact in favor of an excess of Ce. However, the metal-to-iodine distances are somewhat short for Ce^{3+} if one compares to the sum of ionic radii of Ce^{3+} (1.01 Å) and I^- (2.20 Å). Ce^{4+} in an iodide can be ruled out for chemical reasons. In conclusion, a definite decision about the occupation of the 3*a* position cannot be made at present.

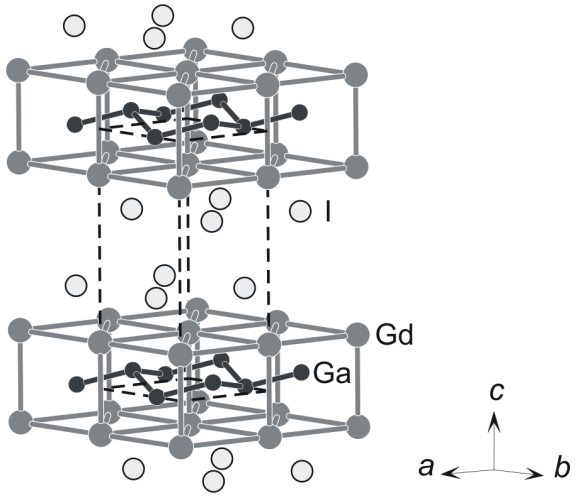

Fig. 3. The $Gd_2I_2Ga_2$ structure viewed approximately along [110]. It consists of one I-Gd-(GaGa)-Gd-I layer per unit cell.

The compounds $Gd_2I_2Ga_2$ and $Y_2I_2Ga_2$ crystallize in the space group $P\bar{3}m1$ (Fig. 3) and are isostructural to $Ce_2I_2Si_2$ and $La_2I_2Ge_2$ [3, 12]. We will focus our discussion on the Gd compound. The Ga-centered Gd_6 trigonal prisms are condensed into a two-dimensional layer in the same fashion as for the previously discussed Ce compounds. The only difference lies in the stacking of these layers. In $Gd_2I_2Ga_2$ the I-Gd-(GaGa)-Gd-I layer stacks on top of the previous one without the shift of the I sheet as in the Ce compounds. Thus the lattice type is primitive and the cell volume is 1/3 of that of the rhombodedral lattice of the Ce compounds. Because of this direct stacking, the distance from the center of the void between the I layers

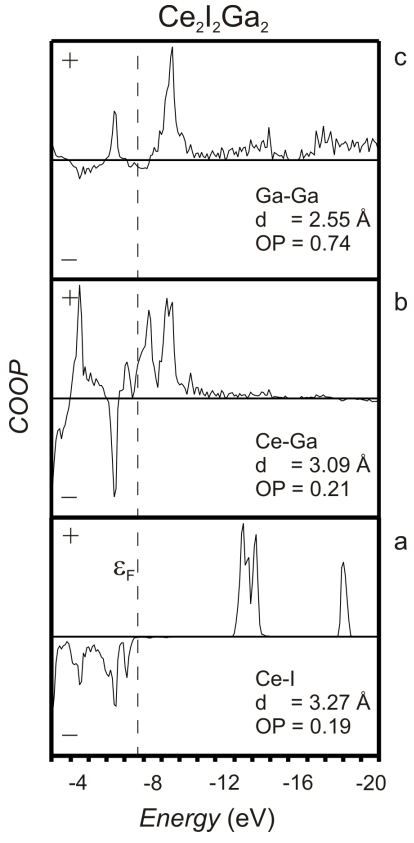

Fig. 4. EH COOP curves for representative bonds in $Ce_2I_2Ga_2$ calculated for a stoichiometric compound. The + region is the bonding area and the − region the antibonding area. The bond type, its distance (d) and integrated overlap population (OP) to the Fermi level are indicated in the panels. The dashed vertical line is the Fermi level.

to a nearest Gd atom is 3.684 Å. This distance would likely be too short for an occupation of the void by an additional metal atom. The Ga node in this honeycomb net is also puckered with the Ga–Ga–Ga angle equal to 115.1°. The Ga–Ga distance is 2.487 Å and the shortest Gd–Gd distance, again along the rectangular edge of the Gd_6 trigonal prism, is 4.108 Å. The shorter Gd–Gd distance compared to that of Ce–Ce is as expected considering the atomic radii.

Electronic structure

For the stoichiometric compounds a formal electron partition as $(RE^{3+})_2(I^-)_2(M^{2-})_2$ implies that they are electron-precise leaving no valence electrons in the *RE* framework. The M^{2-} species of the honeycomb net is valence isoelectronic to N, and a pyramidal configuration at the Al or Ga node is therefore expected from an electronic point of view as well as from the positions of the nearest I atoms. Within this picture, all states below the Fermi level will contribute to bonding as confirmed by the EH COOP curves of representative atom contacts calculated for the stoichiometric $Ce_2I_2Ga_2$ structure shown in Fig. 4. In this figure, the features in the Ce-I COOP curve are relatively sharp, as it is typical for an ionic interaction. The Ga–Ga states spread over a large energy range due to the extended Ga–Ga covalent bonding within and between cells. The features remain essentially the same in a calculation for nonstoichiometric $Ce_{2+x}I_2Ga_2$. Assuming a composition $Ce_2I_2Ga_{2+y}$ (Fig. 5), the Ga1–I antibonding state will be occupied even for $y = 0$ because Ga is more electronegative than Ce. Hence the Ga1–I antibonding states will be lower in energy than those of the Ce1–I interaction. Consequently, the EH calculation also supports the Ce occupancy of the 3*a* site. For $Y_2Br_2Fe_{2+x}$, the *d* orbitals of Fe complicate the matter further and the Fe occupancy is favored [31].

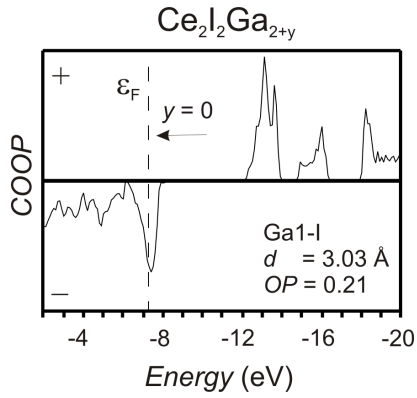

Fig. 5. EH COOP curves for representative bonds for a hypothetical $Ce_{2+x}I_2Ga_{2+y}$ calculated for a full Ga1 occupancy at the 3*a* position ($x = 0$, $y = 1$). The + region is the bonding area and the − region the antibonding area. The bond type, its distance (d) and integrated overlap population (OP) to the Fermi level are indicated in the panel. The dashed vertical line is the Fermi level corresponding to $y = 0$.

The pyramidal configuration at the Al/Ga site in the puckered honeycomb net leaves lone pairs which are clearly seen in the ELF plot in Fig. 6 calculated through the LDA method for the three compounds. However, there is a back donation of electrons especially from the lone pairs to the rare earth metal framework. The EH estimate (usually an overestimate) is 1.3 electrons donated to Ce^{3+} per Ga^{2-} species in the idealized $Ce_2I_2Ga_2$ composition.

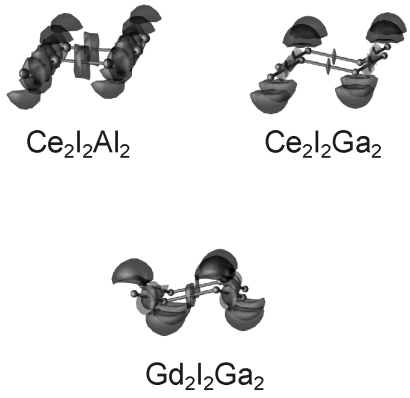

Fig. 6. ELF surface at an isovalue of 0.75, computed by the LDA method for $Ce_2I_2Al_2$, $Ce_2I_2Ga_2$(*i. e.*, $x = 0$, $y = 0$) and $Gd_2I_2Ga_2$. For clarity, only the region of one honeycomb layer is shown.

The question of why $Gd_2I_2Ga_2$ is a stoichiometric compound can not be answered by purely electronic reasons. An occupation of the voids between I atoms results in unreasonably short Gd–Gd contacts, mentioned above as a structural argument. Experiments with La_2I_2Ge could serve as a test case, because it crystallizes in both the $R\bar{3}m$ and $P\bar{3}m1$ space groups at different reaction temperatures, 1050 °C for the former and 1175 °C for the latter [12].

Magnetic and electrical properties

Fig. 7 summarizes the magnetic and electrical properties of $Gd_2I_2Ga_2$ and the nonmagnetic isotypic system $Y_2I_2Ga_2$.

$Y_2I_2Ga_2$ shows the typical decrease of the resistivity with decreasing temperature characteristic of metallic behavior (Fig. 7a). The r. t. resistivity of $Y_2I_2Ga_2$ amounts to about 1 mΩcm and decreases by about one order of magnitude on cooling to liquid-He temperature. The r. t. resistivity of $Gd_2I_2Ga_2$ is about an order of magnitude larger and remains constant down to a temperature of about 100 K. Below this temperature the resistivity starts to grow and undergoes a rapid increase by about two orders of magnitude in a rather narrow temperature interval around 40 K. Below this regime the resistivity starts to level off and saturates at a value of 100 Ωcm at lowest temperatures. We ascribe the rapid growth of the resistivity by two orders of magnitude to a metal-insulator transition. The heat capacity data (Fig. 7b) and the magnetic susceptibility (Fig. 7c) indicate a strong correlation of this transition with magnetic anomalies. The magnetic susceptibility

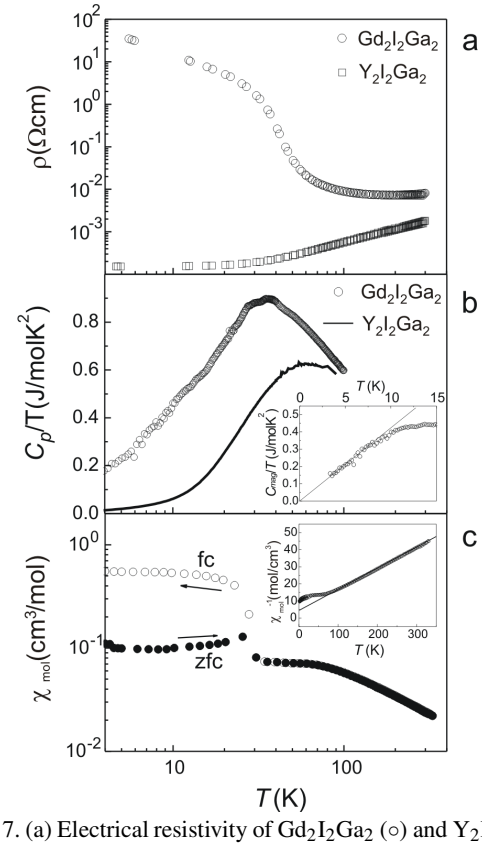

Fig. 7. (a) Electrical resistivity of $Gd_2I_2Ga_2$ (○) and $Y_2I_2Ga_2$ (□). (b) Heat capacities of $Gd_2I_2Ga_2$ (○) and $Y_2I_2Ga_2$ (solid line) normalized to *RE*IGa (*RE* = Ce, Y). The inset shows the magnetic contribution to the heat capacity of $Gd_2I_2Ga_2$. The solid line indicates a power law behavior $C_{mag} \propto T^2$. (c) Field cooled (fc) and zero-field cooled (zfc) magnetic susceptibility of $Gd_2I_2Ga_2$ (per unit GdIGa) determined in a magnetic field of 0.1 T. The arrows show the direction of the temperature change. The inset displays the reciprocal susceptibility measured in a field of 1 T. The solid line represents a Curie-Weiss law with an effective magnetic moment $\mu_{eff} = 8.04\ \mu_B$ and a paramagnetic Curie temperature $\theta = -36$ K. For details see text.

(Fig. 7c) shows a Curie-Weiss behavior (solid line, inset Fig. 7c) with a slope corresponding to an effective magnetic moment of 8.04(3) μ_B consistent with the expected effective moment of 7.93 μ_B for Gd^{3+} with a $4f^7$ electronic configuration and a spin-only $^8S_{7/2}$ ground state. The excess effective moment of 0.1 μ_B corresponds to an excess of about 3 % Gd atoms. The paramagnetic Curie temperature is negative indicating predominant antiferromagnetic exchange interactions and amounts to −36(2) K. Below about 100 K the magnetic susceptibility deviates from the Curie-Weiss behavior due to beginning antiferromagnetic correla-

tions. The low-field magnetic susceptibility (measuring field 0.1 T) reveals a thermal hysteresis characterized by a splitting of the field cooled (fc) and zero-field cooled (zfc) susceptibility branch below about 25 K. The electrical and magnetic anomalies around 100 K are also visible in the magnetic contribution to the heat capacity. $Gd_2I_2Ga_2$ shows an excess heat capacity of magnetic origin which starts to grow below $\sim$ 100 K and becomes clearly visible if we subtract from the heat capacity of $Gd_2I_2Ga_2$ that of $Y_2I_2Ga_2$. The latter can be considered to represent the lattice contributions to the heat capacities, neglecting the 10 % difference due to the different masses of Y and Gd. The thus obtained magnetic contribution to the heat capacity of $Gd_2I_2Ga_2$ is spread over the whole temperature regime below 100 K. There is no sharp (λ-type) anomaly in the heat capacity indicating a transition to a long-range ordered magnetic phase. Rather, a broad maximum is found between 30 K and 10 K, exactly in the temperature regime where the metal-insulator transition is seen in the electrical resistivity. Below $\sim$ 10 K the magnetic heat capacity decreases again according to a power law $C_{\mathrm{mag}} \propto T^2$ common for spin wave contributions of a two-dimensional antiferromagnet. If we integrate C_{mag}/T to obtain the magnetic entropy removed below 100 K we find a value consistent with $\mathrm{R}\,ln(2 \times 7/2 + 1) = 17.3$ J/molK as expected for an S = 7/2 spin system.

The magnetic properties of $Ce_{2+x}I_2Ga_{2+y}$ ($x = 0.06$, $y = 0$ or $x = 0$, $y = 0.11$) (see Fig. 8) show some similarities with that of $Gd_2I_2Ga_2$. Above $\sim$ 150 K the magnetic susceptibility follows a modified Curie-Weiss behavior, $\chi = C/(\mathrm{T} - \theta_{\mathrm{CW}}) + \chi_0$ (solid line, upper inset Fig. 8b) with a negative paramagnetic Curie temperature of $-20(1)$ K and a Curie constant C corresponding to an effective magnetic moment of 2.61(2) μ_{B} which is in fair agreement with the value of 2.54 μ_{B} expected for a free Ce^{3+} ion with a $4f^1$ electronic configuration [32] in a $^2F_{5/2}$ ground state [33]. The excess magnetic moment of 0.07 μ_{B} corresponds to an excess of about 6 %. The diamagnetic contribution γ_0 was estimated from Pascal's increments to -80×10^{-6} cm^3/mol (Ce^{3+}: -20×10^{-6} cm^3/mol; I^-: -52×10^{-6} cm^3/mol; Ga^{3+}: -8×10^{-6} cm^3/mol). Below about 30 K deviations from the Curie-Weiss law are seen which arise either from crystal field splitting effects or from exchange interactions. Below $\sim$ 10 K a sharp increase of the susceptibility is observed when a small external field of 0.01 T is applied. This feature, which is reminiscent of an onset of long-range ferromagnetic or ferrimagnetic ordering with the build-up of a spontaneous magnetization, is readily suppressed by increasing the external field (see lower inset in Fig. 8b) and a normal paramagnetic behavior is restored. In contrast to the low temperature magnetic behavior of $Gd_2I_2Ga_2$, the field cooled and zero-field cooled susceptibilities of $Ce_{2+x}I_2Ga_{2+y}$ show almost no thermal hysteresis.

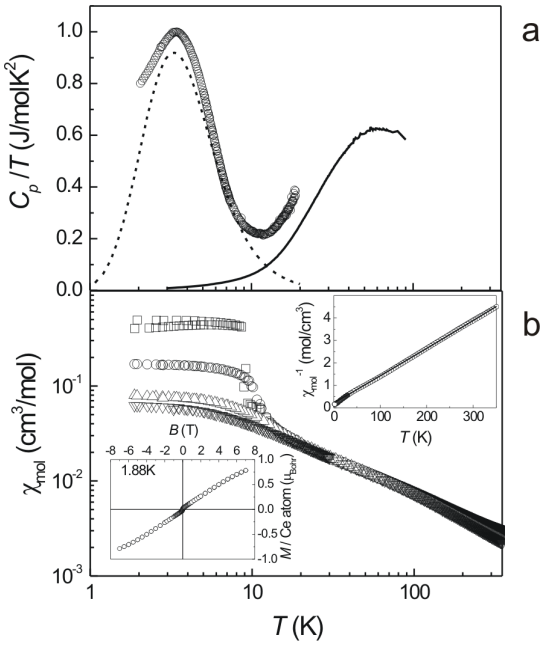

Fig. 8. (a) Heat capacities of $Ce_{2+x}I_2Ga_{2+y}$ (○) and $Y_2I_2Ga_2$ (solid line) normalized to *RE*IGa (*RE* = Ce, Y). The dashed line represents the heat capacity expected for a magnetic two-level system (Schottky anomaly) given by eq. (1). (b) Molar magnetic susceptibilities of $Ce_{2+x}I_2Ga_{2+y}$ measured with increasing magnetic fields (□ 0.01 T, ○ 0.1 T, △ 1 T and ▽ 5 T). The upper inset displays the reciprocal magnetic susceptibility of $Ce_{2+x}I_2Ga_{2+y}$ measured in a magnetic field of 5 T. The solid line represents a Curie Weiss line as described in the text. The slope of the Curie Weiss law corresponds to an effective magnetic moment of 2.61 μ_{B}. The lower inset shows the magnetization of $Ce_{2+x}I_2Ga_{2+y}$ at 1.88 K. The small spontaneous component is readily saturated and paramagnetic behavior is recovered. A noticeable hysteresis is not observed. All data are referred to one half of the formula unit $Ce_{2+x}I_2Ga_{2+y}$ with either $x = 0.06$ and $y = 0$ or $x = 0$ and $y = 0.11$.

The heat capacity of $Ce_{2+x}I_2Ga_{2+y}$ at $\sim$ 10 K shows no *sharp* feature indicative of a transition to a long-range ordered magnetic state. Instead, a *broad* anomaly develops below $\sim$ 10 K. This can be described rather well by a Schottky anomaly expected for thermal exci-

tations across a two-level system. A Schottky anomaly for a two-level system is given by

$$\frac{C_{\mathrm{mag}}}{R} = \left(\frac{\Delta}{k_B T}\right)^2 \frac{\exp\left(\frac{\Delta}{k_B T}\right)}{\left(1+\exp\left(\frac{\Delta}{k_B T}\right)\right)^2} \qquad (1)$$

where R is the molar gas constant and Δ the energy difference between the ground state and the excited state. In Fig. 8a we have plotted the heat capacity according to eq. (1) in comparison with the experimental data assuming an energy separation between the ground and the excited state of *approx.* 11 K.

The origin of such a Schottky anomaly is not fully clear at present. It could be due to an excitation from the ground state doublet to the first excited crystal field doublet. Such an explanation implies that any exchange interaction between the Ce ions is small and essentially single ion behavior is realized. In view of the findings for $Gd_2I_2Ga_2$, where apparent exchange interactions lead to a broadened magnetic contribution to the heat capacity, one could also attribute the Schottky anomaly to an exchange split ground state doublet assuming that the exchange fields from neighboring Ce^{3+}ions are frustrated and long range ordering is suppressed as has been observed for some geometrically frustrated systems [34].

Acknowledgements

We thank Dr. C. Hoch for the intensity data collection, C. Kamella for the EDX measurements, E. Brücher for the magnetic susceptibility measurements, and G. Siegle for the conductivity measurements. C. Z. acknowledges the support by NSF and by the Max-Planck-Gesellschaft which made his visit at MPI possible.

[1] A. Simon, Hj. Mattausch, G. J. Miller, W. Bauhofer, R. K. Kremer in *Handbook on the Physics and Chemistry of Rare Earths*, Vol. 15, Eds.: K. A. Gschneider, Jr., L. Eyring), Elsevier Science Publishers, Amsterdam, **1991**, pp 191 – 285.
[2] Hj. Mattausch, O. Oeckler, A. Simon, *Inorg. Chim. Acta* **1999**, *289*, 174.
[3] Hj. Mattausch, A. Simon, *Angew. Chem.* **1998**, *110*, 498; *Angew. Chem. Int. Ed.* **1998**, *37*, 499.
[4] J. D. Corbett, *J. Chem. Soc., Dalton Trans.* **1996**, 575.
[5] T. Hughbanks, G. Rosenthal, J. D. Corbett, *J. Am. Chem. Soc.* **1986**, *108*, 8289.
[6] T. Hughbanks, J. D. Corbett, *Inorg. Chem.* **1988**, *27*, 2022.
[7] T. Hughbanks, J. D. Corbett, *Inorg. Chem.* **1989**, *28*, 631.
[8] K. Ahn, B. Gibson, R. K. Kremer, Hj. Mattausch, A. Stolovits, A. Simon, *J. Phys. Chem. B* **1999**, *103*, 5446.
[9] C. Zheng, O. Oeckler, Hj. Mattausch, A. Simon, *Z. Anorg. Allg. Chem.* **2001**, *627*, 2151.
[10] H.-Y. Zeng, H. Okudera, C. Zheng, Hj. Mattausch, R. K. Kremer, A. Simon, *Z. Naturforsch.* **2005**, *60b*, 499.
[11] H.-Y. Zeng, M. Lukachuk, H. Okudera, C. Zheng, Hj. Mattausch, A. Simon, *Z. Anorg. Allg. Chem.* **2007**, submitted.
[12] Hj. Mattausch, C. Zheng, M. Ryazanov, A. Simon, *Z. Anorg. Allg. Chem.* **2005**, *631*, 302.
[13] A. Simon, *J. Appl. Cryst.* **1970**, *3*, 11.
[14] G. M. Sheldrick, SHELXTL (version 5), Siemens Analytical Instruments Inc., Madison, Wisconsin (USA) **1994**.
[15] A. Altomare, M. C. Burla, M. Camalli, G. L. Cascarano, C. Giacovazzo, A. Guagliardi, A. G. G. Moliterni, G. Polidori, R. Spagna, *J. Appl. Crystallogr.* **1999**, *32*, 115.
[16] J. Rodriguez-Carvajal, FullProf 2k (version 2.70), CEA-CNRS, Gif-sur-Yvette (France) **2004**.
[17] S. D. Wijeyesekera, R. Hoffmann, *Organometallics* **1984**, *3*, 949.
[18] M. H. Whangbo, R. Hoffmann, R. B. Woodward, *Proc. R. Soc. London* **1979**, *A366*, 23.
[19] R. Hoffmann, *J. Chem. Phys.* **1963**, *39*, 1397.
[20] O. K. Andersen, O. Jepsen, *Phys. Rev. Lett.* **1984**, *53*, 2571.
[21] S. Satpathy, O. K. Andersen, *Inorg. Chem.* **1985**, *24*, 2604.
[22] T. F. Fässler, A. Savin, *Chem. Unserer Zeit* **1997**, *31*, 110.
[23] M. E. Alikhami, Y. Bouteiller, B. Silvi, *J. Phys. Chem.* **1996**, *100*, 16092.
[24] A. D. Becke, K. E. Edgecomb, *J. Chem. Phys.* **1990**, *92*, 5397.
[25] A. Savin, A. D. Becke, J. Flad, R. Nesper, H. Preuss, H. G. von Schnering, *Angew. Chem.* **1991**, *103*, 421; *Angew. Chem. Int. Ed.* **1991**, *30*, 409.
[26] A. Savin, H.-J. Flad, J. Flad, H. Preuss, H. G. von Schnering, *Angew. Chem.* **1992**, *104*, 185; *Angew. Chem. Int. Ed.* **1992**, *31*, 185.
[27] A. Savin, R. Nesper, S. Wengert, T. F. Fässler, *Angew. Chem.* **1997**, *109*, 1892; *Angew. Chem. Int. Ed.* **1997**, *36*, 1808.
[28] B. Silvi, A. Savin, *Nature* **1994**, *371*, 683.
[29] L. J. van der Pauw, *Philips Res. Rep.* **1958**, *13*, 1.
[30] W. Schnelle, E. Gmelin, *Thermochim. Acta* **2002**, *391*, 41.

[31] M. Ruck, A. Simon, *Z. Anorg. Allg. Chem*. **1993**, *619*, 327.

[32] J. H. van Vleck, *The Theory of Electric and Magnetic Susceptibilities*; Oxford University Press, London, **1965**.

[33] P. W. Selwood, *Magnetochemistry*, 2nd ed., Interscience, New York, **1956**.

[34] N. P. Raju, E. Gmelin, R. K. Kremer, *Phys. Rev. B* **1992**, *46*, 5405.